

Three-dimensional dynamic analysis of observed mesoscale eddy in the South China Sea based on complex network theory

YAN-HUI WANG^{1,2}, XIN-RUI SHEN¹, SHAO-QIONG YANG^{1,2(a)} and ZHONG-KE GAO³

¹ Key Laboratory of Mechanism Theory and Equipment Design of Ministry of Education, School of Mechanical Engineering, Tianjin University - Tianjin 300072, China

² The Joint Laboratory of Ocean Observation and Detection, Pilot National Laboratory for Marine Science and Technology - Qingdao, Shandong 266237, China

³ School of Electrical and Information Engineering, Tianjin University - Tianjin 300072, China

received 12 November 2019; accepted in final form 6 January 2020

published online 6 February 2020

PACS 05.45.Tp – Time series analysis

PACS 89.75.Fb – Structures and organization in complex systems

Abstract – Mesoscale eddies have drawn extensive attention due to their central role in ocean energy and mass transport. From July to August 2017, we launched thirteen *Petrel-II* underwater gliders developed by the Tianjin University, China, in the South China Sea to observe a mesoscale eddy and obtain relatively complete three-dimensional (3D) data. The complex network methodology is advanced to construct a novel Ocean Observation Complex Network (OOCN) with multilayer structure, based on the continuous observation data with higher resolution acquired by *Petrel-II* gliders. The hierarchical structure of the mesoscale eddy is obtained, which partly validates the three-compartment structure of the eddy. A number of interesting results shows that the dynamic structure analysis can be carried for mesoscale eddies and other complex ocean phenomena.

Copyright © EPLA, 2020

Introduction. – Mesoscale eddies are ubiquitous and highly energetic phenomena in the ocean, which constitute a crucial cog in oceanic transports [1,2]. They possess features of coherent rotating structure and variability in temporal and spatial scales, with a time scale of weeks to years, and the horizontal scale of tens to hundreds of kilometers [3]. Since they were first discovered in the 1960s, mesoscale eddies have been widely researched, because their migration is often accompanied by the transport of fluid parcels and the distribution of natural marine resources [4,5].

Early on, the limited marine hydrographic survey database was a great obstacle to the incipient research of mesoscale eddies. During the past 20 years when satellite remote sensing was rapidly developed and sea level anomaly satellite observations were greatly collected, the study on the basic characteristics of mesoscale eddies has made rapid progresses [6–8]. Based on the satellite measurements, He *et al.* [9] first reported the essence of Sulu Sea eddies. Kubryakov and Stanichny [10] proposed an automated eddy identification method to

investigate the mesoscale eddy dynamics in the Black Sea. Meanwhile, eddy detection techniques have become increasingly beneficial to the estimate of eddy kinetic energy, vorticity and deformation rate [11,12]. Moreover, sea surface height data and sea level anomaly data have been used to identify and track eddies and study mesoscale features in global oceans [13,14].

Nonetheless, due to the little knowledge about their three-dimensional (3D) dynamic characteristics, we still have limited understanding of oceanic eddies' generation and dissipation mechanisms, which makes a great concern. To address the difficulty in exploring 3D features of eddies, Lin *et al.* [15] proposed a 3D eddy detection scheme to validate a model with observational data. To overcome the lack of systematic full water-depth measurement, Zhang *et al.* [16] designed and actualized the South China Sea Mesoscale Eddy Experiment, which lasted for months. Beyond that, numerical model simulation has become a common and relatively reliable method to detect mesoscale characteristics [17,18]. Some other studies have also used similar methods and achieved certain achievements [19]. In these studies, numerous average structures have been restructured due to the lack of systemic

^(a)E-mail: shaoqiongy@tju.edu.cn

observations of a single eddy. In order to attain average structures, all eddies need to have similar 3D structures. Additionally, because the consummate constraint conditions are not available in the simulation, the promotion of computing capacity leads to the increase of false positive probability.

Therefore, our cognition of 3D eddy structures is restricted by the scarce systematic full water-depth measurements. As a kind of special autonomous underwater vehicle, the underwater glider is an emerging ocean monitoring technology and has become a significant guarantee for the research of ocean science. The first generation of underwater gliders in China was developed by the Tianjin University in 2002, and then the motor pattern and stability of hybrid underwater glider have been analyzed systematically [20]. Therewith, the Tianjin University has developed a series of underwater gliders named *Petrel*, which have got comparable properties to those of their international counterparts. After many years of continuous development, *Petrel-X* glider successfully dived to 8213 m in April 2018, creating the new world record [21]. Meanwhile, the *Petrel-II* hybrid underwater glider has performed an extensive flight-test program to validate its system design and development, showing obvious advantages in the working depth and submerged speed [22,23]. Thereinto, Liu *et al.* [24] obtained and analyzed the underwater noise spectrum, using the underwater noise data measured by *Petrel-II*. Currently, *Petrel-II* has become a basic tool for ocean exploration, which is widely applied to capture ocean phenomena such as internal solitary waves, internal waves and so on [25,26]. In short, *Petrel* gliders can realize continuous observation and detection in a long range and at a large scale in the complex ocean environment, and apply to mesoscale and submesoscale ocean dynamic process monitoring [27].

Presently, there exist three types of eddy detection algorithms, including the algorithms based on physical parameters, those based on flow geometry, and the synthesis algorithms that combine the former two [28–30]. The Okubo-Weiss detection method based on a physical parameter W is one of the widely used and practical methods for eddy detection. However, the threshold W needs to be adjusted constantly according to swirl characteristics of the velocity field. Moreover, the winding-angle method, which belongs to the synthesis algorithm, is an accurate and rapid method [31]. Both kinds of the algorithms are widely used to build the 3D structure of mesoscale eddies and reconstruct the average structure. In view of the observation data of a single eddy, the detection method based on physical parameters is undoubtedly more intuitive and convenient to observe and analyze the 3D structure of ocean eddies.

The South China Sea is one of the largest marginal seas in the Pacific Ocean. Among the global oceans, the northern South China Sea embraces the most active mesoscale eddies, and this in turn has attracted a consortium of academics and scientists to examine their the characteristics

and structures [32]. From July to August 2017, thirteen *Petrel-II* gliders were deployed successively in the South China Sea for continuous observation of a mesoscale eddy. Thus, a novel approach is required to realize the multi-source information fusion and multivariate nonlinear time series analysis for the research of a single mesoscale eddy.

In the current Big Data time, the multi-information fusion analysis in complex networks has become a frontier research topic in the world. Due to their remarkable importance, the complex network methods dedicated to multivariate time series analysis are attracting increasing attention, in areas including language translation system [33], brain network [34], climate network [35], manufacturing information systems [36] and multiphase flows [37,38], etc. Gao *et al.* [39] reviewed the research progress of complex network analysis of time series, and listed some prevalent but also more recently developed methodologies. Then they proposed a novel wavelet multiresolution complex network for analyzing multivariate nonlinear time series, which allows characterization of the nonlinear flow behavior underlying the transitions of oil-water flows [40]. Based on the existing research results, a further study should be carried out to analyze marine multivariate nonlinear time series data and visualize the internal characteristics of eddies, which is of great value to the oceanic circulatory system.

Additionally, multilayer networks have become a leading technology in the network science research field during the recent years [41]. This research has provided methods and theories to support the study of network evolution over time [42,43]. In this paper, a new Ocean Observation Complex Network (OOCN) with multilayer structure is proposed to detect and analyze ocean eddies, based on high-resolution hydrologic data stemmed from *Petrel-II* underwater gliders. It puts emphasis on the research of the 3D structure of mesoscale observations to visualize the internal density variation of water mass and track eddy properties. A new weight matrix is derived for evaluating eddy current characteristics, using the network modularity as a quality metric. By using k-core decomposition, the multilayer structure of the observed mesoscale eddy is deconstructed, and the properties of inner flow are also visualized. The proposed OOCN can capture and analyze the horizontal and vertical motions of different networks, and provide the ability to complete this challenging task. This study provides some new insights into the research of complex ocean phenomena such as mesoscale eddies.

Ocean observation data acquisition with *Petrel-II* underwater gliders. – From July to August 2017, thirteen *Petrel-II* gliders were deployed successively in the South China Sea for continuous observation of a mesoscale eddy. *Petrel-II* adjusts its buoyancy to sink or rise following a zigzag trajectory, and achieves buoyancy change by repeatedly transporting hydraulic oil between the inner tank and the external bladder. By using a GPS navigation device, *Petrel-II* makes communication with the

Iridium satellite system once it rises to the surface. When it goes into deep water, which causes GPS invalidation, a coupled TCM3 digital compass (PNI Sensor Corporation, Santa Rosa, California, USA) and a pressure sensor (KELLER Company, Winterthur, Switzerland) will provide guidance. The gliders carry a conductivity, temperature, and depth sensor (CTD) (Seabird Electronics, Inc., Bellevue, Washington, USA), whose sampling frequency is set at 1 Hz so that vertical resolution of thermohaline stratification amounts to 0.15 m. *Petrel-II* has completed a large number of ocean observations, proving its reliability and excellence [23,25,27].

With the satellite altimeter data, the approximate location of the target mesoscale eddy in the northern South China Sea is obtained, and thus underwater gliders can be deployed based on altimeter statistical results. In combination with the natural situation, the underwater gliders were systematically deployed to track the position and variation of the mesoscale eddy and ensure the comprehensiveness of data collection. In addition, the sailing speed of *Petrel-II* would be 0.5 knots, about 22 km per day, while the propagation speed of mesoscale eddies is only 0.1 m/s, about 8.64 km per day [44]. Thus, the mesoscale eddy can be regarded as being relatively stationary to underwater gliders. That is to say, the relative motion between them will not introduce errors in data sampling. After simple elimination of outliers, the SOCIB Glider Toolbox is used for secondary processing of the entire mesoscale eddy data processing [45].

Construction of the ocean observation complex network. – The analysis of ocean water mass is one of the important subjects in physical oceanography, which could be the final destination of oceanographic research. The pervasive application of ocean equipment for continuous observation has initiated a new stage in the cognition of ocean water masses. The mesoscale eddies, as a breakthrough in the understanding of ocean circulation, can be analyzed as water masses. When internal characteristics of the mesoscale eddy are deconstructed with water mass analysis, it can be seen that the mesoscale eddy is composed of various seawater micelles, whose basic unit is water type. Besides, movements of the seawater micelles cause the formation, evolution and extinction of mesoscale eddies. Hence, this study adopts a new perspective to build the complex network of mesoscale eddy, and examines how its internal network nodes are connected to form a super network. In this section, a unique OOCN is proposed and its system flowchart is shown in fig. 1.

Based on the oceanographic data collected by *Petrel-II*, a 10-layer network is constructed to analyze the characteristics of mesoscale eddies at different depth layers. The depth of these 10 networks ranges from 50 m to 500 m, with a spacing of 50 m, and the thickness of a single layer network is 5 m. Since the sampling frequency of the on-board sensors is set to 1 Hz, the oceanic data of the mesoscale eddy have an equal time interval. In fact, multisource data

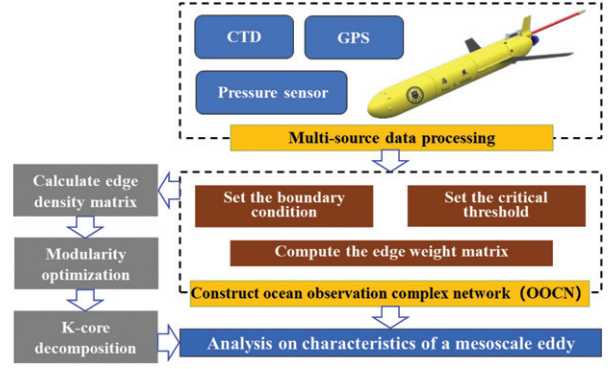


Fig. 1: System flowchart of the OOCN.

of the OOCN is derived from GPS navigation devices, digital compasses, pressure sensors, main processor unit and CTD sensor.

Suppose the sea area under investigation be mapped to X , where m hydrological data are observed, as defined below:

$$X = \{T_1, T_2, \dots, T_m\}. \quad (1)$$

Each water type T_i , as originally defined, is described by potential temperature θ and salinity S . Generally, the distribution of currents in the ocean is dependent on the pressure distribution, which further depends on the variation of the ocean density [46]. According to this, the movement of currents could be tracked by measuring θ and S . Here, we add pressure p to T_i , and calculate bit density ρ_i to characterize T_i and investigate exactly the movement of seawater micelles:

$$T_i = \rho_i(\theta_i, S_i, P_i). \quad (2)$$

Representing type T_i by nodes and bit density difference between nodes by links, the OOCN can be modelled by a weighted network as follows:

$$w_{ij} = \frac{|\rho_i - \rho_j|}{d_{ij}}, \quad (3)$$

where d_{ij} is the Euclidean distance between nodes T_i and T_j . Given the comprehensive information of the gliders' operational profile characteristics, the isotropy and anisotropy of water type, and the spatial continuity of seawater micelles, we adopt a critical threshold $r_c = 3000$ m, and obtain the network connections: an edge connecting nodes T_i and T_j exists if $|d_{ij}| \leq r_c$, while there is no edge between them if $|d_{ij}| > r_c$.

In order to quantify the directionality of the OOCN, the nodes with small bit density are set to point to those with high bit density. As the increase or decrease of seawater micelles density could result in vertical convection, the movement of the micelles can be tracked by comparing the bit density differences between nodes.

Although the network has been preliminarily constructed, it is necessary to optimize the network link and

determine the optimal link density to achieve the best division of seawater micelles. Then, a measurement shall be carried out to evaluate the division of seawater micelles in water mass. From this view, we adopt a modification of modularity algorithm [47] to calculate the modularity under different link densities, and select the optimal value to attain the ideal community structure.

In order to start with a state in which each node in the network is the sole member of a module i , the initial network modularity Q can be computed as

$$Q = \sum_{a_i} (e_{ii} - a_i^2), \quad (4)$$

where e_{ii} (0 initially) is the fraction of all edges that connect vertices within module i , a_i is the proportion of links within the module i (degree of the module i) over the total number of network links [47].

The modularity acts as the standard to measure the quality of community division. The range of Q is 0–1. When the value of Q is relatively high enough, it makes an ideal division of the network. In view of this, we calculate the corresponding modularity under different link densities in an attempt to find the optimal solution for network at each layer. The Q values of networks constructed at different layers show a slight fluctuation, and the calculation results present a weak downward trend with depth. However, the Q values of complex networks constructed at all 10 layers are quite close, all around 0.9. To sum up, the complex network algorithm is compatible with the structure of the mesoscale eddy.

Analysis on characteristics of a mesoscale eddy.

– Based on the data collected by gliders, the OOCN with multilayer structure is constructed for a mesoscale eddy. The network analysis on the multilayer network is performed, and then NetDraw visual software is used to visualize the topological properties of the different layers. The greater the node degree, the higher the degree centrality, and the more important the node is in the network. By making degree centrality analysis, the volume of important nodes is enlarged, while by comparison, the relatively less important nodes are reduced in size, as shown in figs. 2–5. By this stage, the nodes are displayed according to the centrality results, and the size of the nodes reflects the magnitude of node degree and proves a significant internal characteristic of the eddy.

The structure of the OOCN stems from the complexity of ocean water mass. Water masses are composed of multiple seawater micelles with different properties, allowing their growth, coalescence, division and death. The basic unit of seawater micelle is the water type. It is known that the movement of seawater can be characterized qualitatively by seawater density variations. When the densities of two seawater micelles are different, relative movement occurs. In the meantime, adjacent water types are likely to maintain the same motion state, due to the energy dissipation in the process of seawater micelle movements.

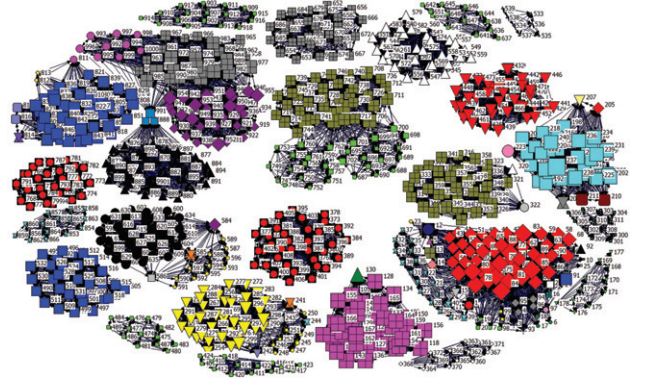


Fig. 2: Community structure of the first layer network. In this network, the k -core values of seawater micelles are 6, 10, 11, 12, 13, 14, 15, 30, 32, 35, 36, 37, 41, 42, 43, 44, 45, 46, 47, 51, and 64. The primary reason, which results in the long span of the k -core, is the interaction between influencing factors of sea surface and the mesoscale eddy.

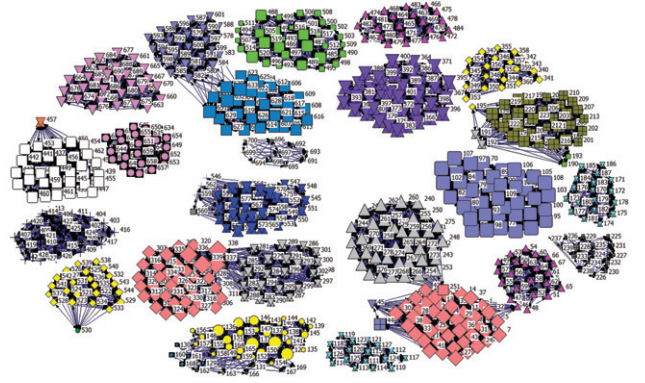


Fig. 3: Community structure of the third layer network. The k -core values of seawater micelles are 5, 6, 7, 8, 9, 10, 11, 13, 14, 15, 16, 17, 18, 19, 20, 21, 22, 23, 24, 26, 27, 28, 29, 31, 33, 36, 38, and 39. Compared with the first two networks, the number of communities in this layer starts to decrease as the surveying depth exceeds 150 meters.

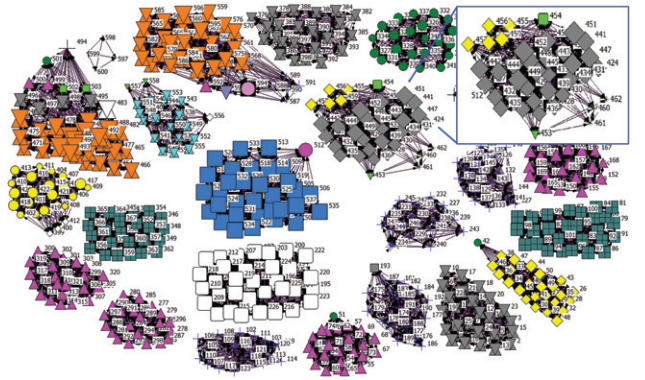


Fig. 4: Community structure of the sixth layer network. The k -core values of seawater micelles are 7, 9, 10, 12, 13, 14, 15, 16, 17, 18, 19, 20, 21, 22, 23, 24, 25, 26, 27, 28, 30, and 31. The community structure of the OOCN is detected by k -core decomposition which reveals the interior flow complexity of water mass.

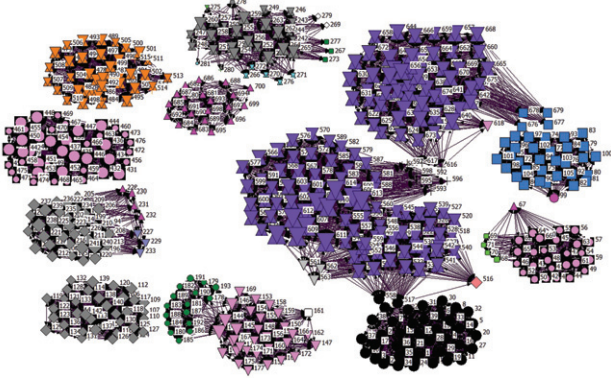


Fig. 5: Community structure of the ninth layer network. The k -core values of seawater micelles are 9, 10, 12, 13, 14, 15, 16, 20, 21, 23, 24, 25, 26, 27, 28, 29, 30, 31, 34, 36, 37, and 38. In this layer network, the community volume obviously increases, showing that this water layer keeps in a relatively stable state.

The water type may be affected by its new environment and change its state of motion over a definite distance. This precisely reflects the isotropy and anisotropy of seawater micelles. Given the anisotropy of the seawater micelles, the directionality of the considered networks can be quantified, as shown in the local magnification of fig. 4. The organigram of each layer network presents uniform structural characteristics, namely that every network is divided into numerous substructures. The miscellaneous colors and shapes are used to classify the nodes with different characteristics. Nodes with the same characteristics tend to aggregate into one substructure and are separated from nodes with different ones, which reflects the isotropy and anisotropy of the OOCN. This is also because the composition of substructures depends on the constraint of the edge condition and node degree in addition to the k -core constraint. A few “nodes” with different characteristics may be partly the change agent of growth and extinction process of substructures. Thus, a community containing sporadic nodes with different attributes is not the result of misclassification, but a precise embodiment of isotropy and anisotropy of water mass. This shows that OOCN can effectively fit the complex physical reaction of the eddy and has a very high correspondence with the complex ocean phenomena.

The k -core decomposition is now a key tool for visualization of complex networks and explanation of internal transformations. The k -core could be realized by removing all vertices less than k degree from the network, until there are no more to remove. As a result, k -cores are a set of nodes that are connected more closely to each other internally. In other words, k -cores are a “group” or “substructure” of nodes. The degree distribution of networks basically determines the structure of the k -cores, and the following formula can be used [48]:

$$M(k) = p \sum_{q \geq k} P(q) \sum_{n=k}^q C_n^q R^{q-n} (1-R)^n, \quad (5)$$

where $M(k)$ denotes the probability of a node in the k -core, $P(q)$ is a random configuration model with a given degree distribution, k generally counts from 1 in this equation, and R is the probability that an endpoint of the edge is the root of the k -core. To make sure one end of an edge is not a root of an infinite $(k-1)$ -ary substructure, subbranches of $k-2$ at the utmost are roots of infinite $(k-1)$ -ary substructure. In this case, R should be expressed here formulaically:

$$R = 1 - p + p \sum_{n=0}^{k-2} \left[\sum_{i=n}^{\infty} \frac{(i+1) P(i+1)}{z_i} C_n^i R^{i-n} (1-R)^n \right], \quad (6)$$

where $z_i = \sum_q q P(q)$ is the mean number of the nearest neighbors of a node in the network, and n starts from $k-2$ at most.

The k -core is an inner circle of the network structure. The vertices less than k degree form plentiful finite groups whose degrees of vertices are $q \geq k$ and do not belong to the k -core. These clusters are either connected to the k -core by less than k edges or isolated from it. This explains why substructures of the OOCN have a few nodes with different characteristics and reflects the anisotropy of the seawater micelles in the water mass. Then we calculate the k -core values of the 10-layer networks and use corresponding colors to represent nodes with different k -core values. Based on the calculation methods of edge connection strategy, the edge weight and k -core in networks at different depth layers are unified. It is ensured that nodes in all layers with the same color and shape have certain identical properties. Accordingly, we can analyze the internal motions of the mesoscale eddy by observing the distribution and change of seawater micelles in each layer network.

Furthermore, as shown in figs. 2–5, the number of seawater micelles decreases in the layer network as the depth increases. The emergence of this phenomenon is most likely caused by factors such as the movement of the wind-drift surface that affects the upper parts of the mesoscale eddy. By k -core decomposition, the distribution of seawater micelles at different depths could be clearly illustrated. Networks at all ten layers have some seawater micelles with the same magical k -core properties. It can be seen that seawater micelles of each layer have continuity, meaning that the OOCN decomposes seawater micelles into equal depth slices. The individual layers of the OOCN can be thought of as randomly damaged uncorrelated networks which can be characterized as k -cores. The k -core as the continuously confined substructure is the largest subgraph in which the vertices have at least k interconnects. It is surprising to find that the visualization of the water mass stratification shows the position and size of the seawater micelles at different depths. By connecting the positions of the seawater micelles with the corresponding color and shape in each layer, the dynamic 3D diagram of the mesoscale eddy could be constructed. In other words, this

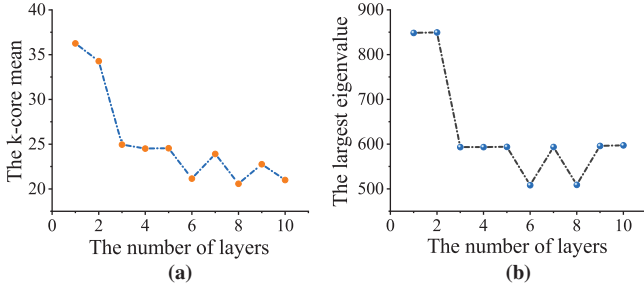


Fig. 6: Hierarchical structure of the mesoscale eddy.

intuitively reflects the horizontal and vertical motions of seawater micelles with different properties.

The above statistics correspond to the network centrality analysis in the complex network algorithm. Then the k -core mean value is calculated as shown in fig. 6(a) and consensus analysis of each layer network is performed as shown in fig. 6(b). Due to the agitation of winds and waves, an intensive mixing layer is formed at the ocean surface. In the mixed layer, the first two layer networks exhibit strong isotropy of seawater micelles in a certain region. Simultaneously, the anisotropy of seawater micelles in the first two layer networks is strongly influenced by disorder and frustration of the interaction between influencing factors, which makes the k -core mean value a little high. As displayed, k -core mean value plunged from the second to third layers. A similar trend is found in the consensus analysis that the largest eigenvalues reduced quickly between 100 and 150 m. Thus, the large eigenvalue indicates a good fit to the consensus model and embodies the hierarchical structure of mesoscale eddies.

As illustrated in fig. 7(a), the community numbers of each layer network are presented. In the latter two layers, the community number is significantly reduced, and the scale of seawater micelles with the same properties is enlarged, which may help to form a certain equilibrium state. Since the bit density fluctuation can indirectly characterize the change of marine drift, it is necessary to take into account the edge weight value in eq. (3). Moreover, fig. 7(b) shows the edge average weight value and edge weight bias of 10-layer networks, which present a consistent declining trend. The edge weight bias drops extremely from the first layer to the second layer, and then keeps a steady decreasing trend. It is noticeable, however, that the edge weight bias of the first layer network is very large, which is caused by the disturbed surface water in mixed layers. Then fig. 7(b) takes on obvious stratification, which may be caused by the coupling of seawater movement, diffusion and mixing in the ocean-atmosphere system. Remarkably, the hierarchical structure of the OOCN corresponds to the three-compartment structure of the mesoscale eddy, which was found by Zhang *et al.* [49]. Thereinto, the average weight value in the 10th layer approaches 0, which is most likely the characteristic of the mode water layer.

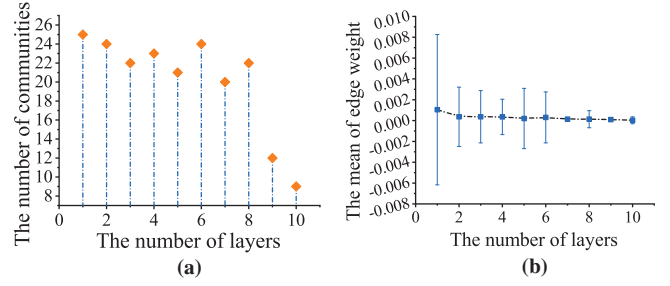


Fig. 7: Variation tendency of the 10-layer networks.

These results indicate that the complex network algorithm is ideal for dynamic analysis of complex ocean eddies. The OOCN has high accuracy for the network division of water mass, and can realize the 3D tracking of anisotropic seawater micelles in mesoscale eddies. If underwater gliders can perform real-time analysis of the observed ocean phenomena according to the algorithm in this paper, the findings may have certain guiding significance for the formation control of underwater gliders with the task of ocean observation.

Conclusion. – The research on the mesoscale eddy generation, propagation and extinction mechanisms is still an important but highly challenging topic in the field of marine science, due to the lack of continuous observation data with higher resolution to reflect the real 3D structure of mesoscale eddies. To address the problem, we used the altimeter data to locate the mesoscale eddy position, and then launched thirteen Chinese *Petrel-II* gliders in the South China Sea to continuously observe a mesoscale eddy, from July to August 2017. Based on the multi-source data obtained from *Petrel-II* gliders, a novel OOCN with multilayer structure is proposed to describe dynamic characteristics of a mesoscale eddy at different depths. The layered structure and three-compartment structure are deconstructed, which are both important indicators of mesoscale eddies to characterize seawater micelles of different characteristics. Besides this, the mesoscale eddy is reconstructed by complex network theory and water mass analysis, and the internal horizontal and vertical motions of this reconstructed mesoscale eddy are revealed as well, which has proven that the OOCN is one of the effective tools for the study of complex ocean phenomena. Furthermore, future work will focus on how to combine balanced dynamics of mesoscale eddies with complex network nonlinear dynamics to analyze the dissipation law of mesoscale eddies and achieve the prediction of energy dissipation mechanism, based on the extended relational agro-statistics data.

This work was jointly supported by National Key R&D Program of China (Grant Nos. 2016YFC0301100 and 2017YFC0305902) and the Research Funds from Shenzhen Investment Holdings Company Limited; National Natural

Science Foundation of China (Grant Nos. 51721003, 51722508, 11902219 and 61922062); Natural Science Foundation of Tianjin City (Grant Nos. 18JCQNJC05100 and 18JCQJC46400); Aoshan Talent Cultivation Program (Grant Nos. 2017ASTCP-OS05 and 2017ASTCP-OE01) of QNLM; the Marine S&T Fund of Shandong Province for Pilot National Laboratory for Marine Science and Technology (Qingdao) (Grant No. 2018SDKJ0205). The authors also would like to express their sincere thanks to L. MA for her helping revise the grammar.

REFERENCES

- [1] ZHANG Z. H., WANG W. and QIU B., *Science*, **345** (2014) 322.
- [2] HOLLAND W. R., *J. Phys. Oceanogr.*, **8** (1978) 363.
- [3] WEISS J. B. and GROOMS I., *Chaos*, **27** (2017) 126803.
- [4] SIEGEL D. A., MCGILLICUDDY D. J. jr. and FIELDS E. A., *J. Geophys. Res.*, **104** (1999) 13359.
- [5] MCGILLICUDDY D. J. jr., *Annu. Rev. Mar. Sci.*, **8** (2016) 125.
- [6] MCGILLICUDDY D. J. jr., ROBINSON A. R., SIEGEL D. A., JANNASCH H., JOHNSON R., DICKEY T., MCNEIL J., MICHAELS A. and KNAP A., *Nature*, **394** (1998) 263.
- [7] GAUBE P., MCGILLICUDDY D. J. jr. and MOULIN A. J., *Geophys. Res. Lett.*, **46** (2019) 1505.
- [8] MELNICHENKO O., AMORES A., MAXIMENKO N., HACKER P. and POTEMRA J., *J. Geophys. Res.: Oceans*, **122** (2017) 1416.
- [9] AMORES A., MONSERRAT S., MELNICHENKO O. and MAXIMENKO N., *Geophys. Res. Lett.*, **44** (2017) 6926.
- [10] KUBRYAKOV A. A. and STANICHNY S. V., *Oceanology*, **55** (2015) 56.
- [11] GULA J., MOLEMAKER M. J. and MCWILLIAMS J. C., *J. Oceanogr.*, **46** (2016) 305.
- [12] MASON E., PASCUAL A. and MCWILLIAMS J. C., *J. Atmos. Ocean. Tech.*, **31** (2014) 1181.
- [13] CHELTON D. B., GAUBE P., SCHLAX M. G., EARLY J. J. and SAMELSON R. M., *Science*, **334** (2011) 328.
- [14] LIEN R.-C., MA B., CHENG Y.-H., HO C.-R., QIU B., LEE C. M. and CHANG M.-H., *J. Geophys. Res.: Oceans*, **119** (2014) 2129.
- [15] LIN X., DONG C., CHEN D., LIU Y., YANG J., ZOU B. and GUAN Y., *Deep-Sea Res. Part I*, **99** (2015) 46.
- [16] ZHANG Z., TIAN J., QIU B., ZHAO W., CHANG P., WU D. and WAN X., *Sci. Rep.-UK*, **6** (2016) 24349.
- [17] ZHANG Z., ZHANG Y. and WANG W., *J. Geophys. Res.: Oceans*, **122** (2017) 1653.
- [18] DONG D., BRANDT P., CHANG P., SCHÜTTE F., YANG X., YAN J. and ZENG J., *J. Geophys. Res.: Oceans*, **122** (2017) 9795.
- [19] BERLOFF P., *Fluids*, **3** (2016) 22.
- [20] NIU W. D., WANG S. X., WANG Y. H., YANG S. and ZHU Y. Q., *China Ocean Eng.*, **31** (2017) 528.
- [21] LI H. Z., WANG Y. H. and WANG S. X., *Sea Technol.*, **60** (2019) 18.
- [22] XUE D. Y., WU Z. L., WANG Y. H. and WANG S. X., *Chin. J. Mech. Eng.*, **31** (2018) 17.
- [23] WANG Y. H. and YANG S. Q., *Glider*, in *Encyclopedia of Ocean Engineering*, edited by CUI W. C., FU S. X. and HU Z. Q. (Springer, Singapore) 2019.
- [24] LIU L., XIAO L., LAN S. Q., LIU T. T. and SONG G. L., *Acoust. Aust.*, **46** (2018) 151.
- [25] MA W., WANG Y. H., YANG S. Q., WANG S. X. and ZHAO X., *J. Coastal Res.*, **34** (2018) 1188.
- [26] QIU C. H., MAO H. B., WANG Y. H., YU J. C., SU D. Y. and LIAN S. M., *J. Oceanogr.*, **75** (2019) 139.
- [27] SHEN X., WANG Y., YANG Q., LIANG Y. and LI H., *J. Unman. Undersea Syst.*, **26** (2018) 89.
- [28] NENCIOLI F., DONG C., DICKEY T., WASHBURN L. and MCWILLIAMS J. C., *J. Atmos. Ocean. Technol.*, **27** (2010) 564.
- [29] OKUBO A., *Deep Sea Res. Oceanogr. Abstr.*, **17** (1970) 445.
- [30] WEISS J., *Physica D*, **48** (1991) 273.
- [31] SADARJOEN I. A. and POST F. H., *Comput. Graph.*, **24** (2000) 333.
- [32] ZHAO R., ZHU X. H. and GUO X., *Cont. Shelf Res.*, **143** (2017) 240.
- [33] SHIMADA Y., TATARA M., FUJIWARA K. and Ikeguchi T., *EPL*, **127** (2019) 56003.
- [34] GAO Z.K., ZHANG K. L., DANG W. D., YANG Y. X., WANG Z. B., DUAN H. B. and CHEN G. R., *Knowl.-Based Syst.*, **152** (2018) 163.
- [35] KANIN E., VAINSHTAIN A., OSIPTSOV A. and BURNAEV E., *EPL*, **193** (2018) 012028.
- [36] SONG Z., SUN Y., YAN H., WU D., NIU P. and WU X., *IEEE Access*, **6** (2018) 3731.
- [37] GAO Z., DANG W., MU C., YANG Y., LI S. and GREBOGI C., *IEEE Trans. Ind. Inform.*, **14** (2018) 3982.
- [38] MOSDORF R. and GÓRSKI G., *Int. Commun. Heat Mass Transfer*, **64** (2015) 14.
- [39] GAO Z. K., SMALL M. and KURTHS J., *EPL*, **116** (2016) 50001.
- [40] GAO Z.-K., LI S., DANG W.-D., YANG Y.-X., DO Y. and GREBOGI C., *Int. J. Bifurcat. Chaos*, **27** (2017) 1750123.
- [41] PERC M., *Eur. Phys. J. ST*, **228** (2019) 2351.
- [42] MAJHI S., PERC M. and GHOSH D., *Chaos*, **27** (2017) 073109.
- [43] MAJHI S., PERC M. and GHOSH D., *Sci. Rep.*, **6** (2016) 39033.
- [44] WU C. R. and CHIANG T. L., *Deep-Sea Res. Pt. II*, **54** (2007) 1575.
- [45] TROUPIN C., BELTRÁN J. P., HESLOP E., TORNER M., GARAU B., ALLEN, J., RUIZ S. and TINTORÉ J., *Methods Oceanogr.*, **13** (2015) 13.
- [46] DEFANT A., *Physical Oceanography*, Vol. **1** (Pergamon, Oxford) 1961.
- [47] DANON L., DÍAZ-GUILERA A. and ARENAS A., *J. Stat. Mech. Theory E*, **2006** (2006) 11010.
- [48] DOROGVTSEV S. N., GOLTSEV A. V. and MENDES J. F. F., *Phys. Rev. Lett.*, **96** (2006) 040601.
- [49] ZHANG Z. G., ZHANG Y. and WANG W., *J. Geophys. Res.: Oceans*, **122** (2017) 1653.